Contrib Mineral Petrol (1998) 131: 379–392

Anne Feenstra · Martin Engi

An experimental study of the Fe-Mn exchange between garnet and ilmenite

Received: 12 September 1996 / Accepted: 11 December 1997

Abstract The exchange equilibrium

$$1/3Fe_3Al_2Si_3O_{12} + MnTiO_3 = 1/3Mn_3Al_2Si_3O_{12} + FeTiO_3$$
almandine pyrophanite spessartine ilmenite

was studied by reversal experiments as a function of temperature ($650 \le T \le 1000$ °C), pressure ($10 \le P \le 20$ kbar), and chemical composition. Experiments were performed in a piston-cylinder apparatus using starting mixtures consisting of 95% garnet and 5% ilmenite. At the lower temperatures, 3–5% PbO flux was added to the reactants. The PbO was reduced to metallic lead by the graphite of the capsules. The EMP analysis shows that ilmenite is essentially a solid solution of $FeTiO_3$ and $MnTiO_3$ with up to 4.5 mol% Fe_2O_3 (for Fe-rich compositions). Garnet is compositionally close to $(Fe,Mn)_3Al_2Si_3O_{12}$ but apparently contains up to 1.0 wt% TiO_2. As garnet was usually analyzed within 5–15 μm distance from ilmenite grains, the Ti measured in garnet appears to be largely an analytical artifact (due to secondary fluorescence). This was confirmed by analyzing profiles across a couple constructed from ilmenite and Ti-free garnet. The more than 100 exchange runs indicate that the distribution coefficient K_D $[= (X_{Mn}^{gnt} \cdot X_{Fe}^{ilm})/(X_{Fe}^{gnt} \cdot X_{Mn}^{ilm})]$ is essentially independent of P and decreases with T. With a few exceptions at Mn-rich compositions, the present results are consistent with previous studies on the Fe-Mn partitioning between garnet and ilmenite. Contrary to previous studies, however, the narrow experimental brackets obtained during the present calibration constrain that, at constant T, K_D is larger for Mn-rich compositions than for Fe-rich ones. This compositional dependence of K_D will complicate garnet-ilmenite geothermometry. Mutually consistent activity models for Fe-Mn garnet and ilmenite, based on a thermodynamic analysis of the present results and other phase equilibria studies in the system $Fe\text{-}MnO\text{-}Al_2O_3\text{-}TiO_2\text{-}SiO_2\text{-}O_2$, will be presented in a following contribution (M. Engi and A. Feenstra, in preparation).

A. Feenstra[1](✉) · M. Engi
Mineralogisch-petrographisches Institut, University of Berne, Baltzerstrasse 1, CH-3012 Berne, Switzerland

Present address:
[1]Geo Forschungs Zentrum Potsdam, Telegrafenberg, D-14473 Potsdam, Germany

Editorial responsibility: V. Trommsdorff

Introduction

Garnet occurs as a rock-forming mineral over a wide range of metamorphic grades and magmatic conditions and therefore is one of the most important phases used in petrogenetic calculations (see e.g., reviews of Essene, 1989, and Spear, 1993). In a vast majority of bulk compositions, the chemical composition of garnet can be approximated in the quaternary system $Fe_3Al_2Si_3O_{12}$-$Mg_2Al_2Si_3O_{12}$-$Mn_3Al_2Si_3O_{12}$-$Ca_3Al_2Si_3O_{12}$ (almandine–pyrope–spessartine–grossular). To obtain accurate geothermobarometric results from phase equilibria involving multicomponent garnet, solution properties derived from experimental work are a prerequisite. Most of these experimental activity-composition (a-X) studies have been restricted to binary garnet joins (e.g., Fe-Mg: Geiger et al. 1987; Hackler and Wood 1989; Koziol and Bohlen 1992; Fe-Mn: Pownceby et al. 1987; Fe-Ca: Geiger et al. 1987; Koziol 1990; Ca-Mn: Koziol 1990; Gavrieli et al. 1996; Mn-Mg: Wood et al. 1994). Some experiments also involved ternary solutions of Fe-Mg-Ca garnets (Koziol and Newton 1989; Berman and Koziol 1991; Ganguly et al. 1996), Fe-Mn-Ca garnets (Pownceby et al. 1991) and Mg-Mn-Ca garnets (Ganguly et al. 1996). Recently, limited experimental work on Fe-Mg-Mn-Ca garnets has been conducted by Koziol (1996) and Ganguly et al. (1996). These ternary and quaternary experimental data provide an important test for the current solution models for Fe-Mg-Mn-Ca garnet (e.g., Ganguly and Saxena 1984; Berman 1990), which are mainly based on the binary experimental data.

Garnet shows pronounced cation fractionation with many silicate and oxide phases. Of these the Fe-Mg fractionation with biotite, first calibrated by Ferry and Spear (1978), is probably the most widely used geothermometer. In metamorphic and magmatic rocks, garnet and ilmenite are the most common phases to concentrate Mn. The Fe-Mn partitioning between these phases may be expressed by the exchange equilibrium

$$1/3Fe_3Al_2Si_3O_{12} + MnTiO_3 = 1/3Mn_3Al_2Si_3O_{12} + FeTiO_3$$
almandine pyrophanite spessartine ilmenite

The temperature dependence of the $K_{D^{gnt-ilm}_{Mn-Fe}}[= (X^{gnt}_{Mn} \cdot X^{ilm}_{Fe})/(X^{gnt}_{Fe} \cdot X^{ilm}_{Mn})]$ was first recognized to have potential as a geothermometer in studies of metapelitic assemblages (e.g., Tracy et al. 1976; Woodsworth 1977; Tracy 1982). Docka (1984) presented a preliminary empirical thermometric calibration of the $K_{D^{gnt-ilm}_{Mn-Fe}}$, based on data obtained from metapelites of New England.

There are three experimental studies that aimed at calibrating equilibrium (1) as a function of P, T and bulk composition. Using oxide starting mixtures, Ono (1980) obtained Fe-Mn partitioning data from synthesis experiments at 950–1050 °C and 5–10 kbar. His results show considerable scatter. Kress (1986) conducted hydrothermal reversal runs in the temperature range 700–1050 °C at pressures of 10, 12 and 20 kbar, with oxygen fugacity controlled by the IW (iron wustite)-buffer. The study yielded fairly wide reversals at the lower temperatures, particularly for Mn-rich bulk compositions. The most extensive study on Fe-Mn partitioning between garnet and ilmenite so far was by Pownceby et al. (1987), who hydrothermally reversed the Fe-Mn partitioning for five different garnet compositions at temperatures of 600–900 °C and pressures of 2 and 5 kbar. Oxygen fugacity was controlled at values of the QFM (quartz magnetite fayalite)-buffer by means of a modified Shaw membrane technique. Pownceby et al. (1987) fitted their Fe-Mn partitioning data by least squares regression to derive $W^G_{Fe-Mn} = 0.9 \pm 1.2$ kJ/mol for garnet (regular solution model), implying very minor positive deviation from ideality along the almandine–spessartine join. The W^G_{Fe-Mn} for garnet was obtained substituting $W^G_{Fe-Mn} = 1.7 \pm 0.2$ kJ/mol for Fe-Mn ilmenite, a value derived from emf measurements on the assemblage Fe-Mn ilmenite + rutile + metallic iron. Though not explicitly stated in their paper, Pownceby et al. (1987) interpreted their partitioning data to indicate that $K_{D^{gnt-ilm}_{Mn-Fe}}$ is independent of composition at constant T (see their Figs. 2 and 3). In a subsequent study, Pownceby et al. (1991) investigated the effect of calcium on the Fe-Mn partitioning between garnet and ilmenite, using starting material consisting of crystallized Fe-Mn ilmenite and Ca-Fe-Mn garnet oxide mixtures seeded with Fe-Mn garnet. From the partitioning data they deduced for garnet $W^G_{Fe-Mn} = 0.62 \pm 0.20$ kJ/cation-mol. Recently, the W^G_{Fe-Mn} of garnet was slightly modified to 539 J/cation-mol (Ganguly et al. 1996).

Although the above experimental studies all agree that $K_{D^{gnt-ilm}_{Mn-Fe}}$ decreases with temperature and is essentially independent of pressure, several discrepancies exist amongst the studies. As outlined by Pownceby et al. (1987; their Fig. 3), the variation of $K_{D^{gnt-ilm}_{Mn-Fe}}$ with temperature (without considering compositional dependence of K_D) as deduced from their partitioning experiments differs markedly from that given by Kress (1986). This difference may in part be related to two facts: (1) many reversals, particularly for Mn-rich bulk compositions, are fairly wide, preventing a precise determination of K_D as a function of T and composition; (2) Kress (1986) did not analyze garnet in his products, whereas Pownceby et al. (1987) failed to analyze them in their starting materials, so that in both cases the direction of reaction is uncertain for runs with minor compositional changes of ilmenite and garnet. Pownceby et al. (1987) also noted that for greenschist- to amphibolite-grade rocks, temperatures deduced from their Fe-Mn garnet-ilmenite thermometer, tend to be 30–150 °C higher than obtained with other phase equilibria and thermometers, particularly with the Fe-Mg garnet-biotite thermometer.

The main experimental goal of the present study was to reverse equilibrium (1) over the entire compositional range of the system, and in part at higher pressures and temperatures than in previous studies. Special attention was given to careful chemical characterization of the starting and final products by electron microprobe (EMP) analysis guided by back-scattered electron (BSE) imaging. The present paper describes the experimental approach used, the chemistry of garnet and ilmenite of the run products, and compares the experimental results with those of previous studies on Fe-Mn partitioning between garnet and ilmenite.

In a following paper (M. Engi and A. Feenstra, in preparation), mutually compatible activity models for Fe-Mn garnet and Fe-Mn ilmenite will be presented. These activity models have been derived from a detailed thermodynamic analysis in the subsystem Fe-MnO-Al_2O_3-TiO_2-SiO_2-O_2, which not only considered the results of the present study but notably included the data of Pownceby et al. (1987) for Fe-Mn garnet-ilmenite partitioning and Feenstra and Peters (1996) for the redox equilibrium $Fe + TiO_2 + 1/2\ O_2 = $ Fe-Mn ilmenite. Furthermore, the data analysis was anchored to an update of Berman's thermodynamic database (Berman and Aranovich 1996), yielding solution model parameters for Fe-Mn garnet and Fe-Mn ilmenite (as well as standard state thermodynamic properties for spessartine and pyrophanite) that are internally consistent with that multicomponent database.

Experimental

Synthesis of starting materials

Garnet synthesis from oxide mixtures is hampered by the slow kinetics of garnet growth. The Fe-Mn garnets were therefore synthesized in two steps following the procedure proposed by Bohlen et al. (1983). First, glass of several stoichiometric garnet compositions was prepared by melting specpure oxide mixes of MnO_2, Fe_2O_3, Al_2O_3 and SiO_2 in thick-walled graphite crucibles with tightly fitting lids, at temperatures in the range 1370–1425 °C. To avoid oxidation of the graphite crucible, the furnace was flooded with Ar gas. We attempted to produce light-green (Fe-rich compositions) or colorless glasses by using reduction times slightly shorter than those at which metallic Fe crystallized from the melt. Glasses of the proper color were finely ground and tightly packed in graphite capsules (≈300 mg) and run in a piston-cylinder apparatus at 920–1000 °C and 20 kbar for 4–8 days. A total of 25 Fe–Mn garnet synthesis runs were carried out to obtain sufficient garnet for the exchange experiments with Fe-Mn ilmenite. Investigations of the charges by microscopy, X-ray diffraction (XRD) and electron microprobe (EMP) indicate that the runs yielded >99% garnet of fairly homogeneous composition (cf., Table 1). Garnet only occasionally contains minor inclusions of quartz, corundum or spinel. A few garnet syntheses showing relatively large variations in X_{Mn} were rejected for usage in exchange experiments with ilmenite. Cation normalization of the EMP data and Mössbauer spectroscopy point to very minor ferric iron in the garnets (Geiger and Feenstra 1993, 1997). Molar volume of mixing data for the almandine–spessartine join derived from the present syntheses (Geiger and Feenstra 1997) indicate a small positive excess volume for the solution, which can be described by a symmetric (Margules) model with $W^v = 0.024\ (\pm 0.005)$ J/(bar · mol).

The Fe-Mn ilmenites were synthesized from oxide mixtures at 1 bar, 900 °C and $\log f_{O_2} = -17.50$ in a gas-mixing furnace equipped with an oxygen-specific electrolyte (Feenstra and Peters 1996). These synthesis conditions yielded binary $FeTiO_3$-$MnTiO_3$ solid solutions.

Fe-Mn exchange between garnet and ilmenite

Exchange experiments were conducted in a conventional piston-cylinder apparatus (Johannes 1978) using a half-inch furnace assembly. The pressure cell consisted of concentric tubes of pyrophyllite, graphite (furnace) and talc. Garnet-ilmenite mixtures were packed into cylindrical graphite capsules (5 mm length, 3 mm OD, 2 mm ID). Three capsules, each filled with ≈40 mg of reactants, were placed in the inner talc cylinder of the furnace assembly in a symmetric way around an axial thermocouple, the end of which is situated at half-height of the capsules. Temperature as measured and controlled by the Pt-$Pt_{90}Rh_{10}$ thermocouple is believed to be accurate to ±5 °C. No correction was made for the effect of pressure on the emf of the thermocouple. The experiments were performed using the piston-in technique. Samples were brought to pressures ≈10% below the final values and then slowly heated to the required temperatures. Pressure increased during this period of heating, but an additional small piston stroke was always necessary to reach the required final pressure. Pressures listed in Table 1 are not corrected for instrumental friction effects.

Experiments were performed at 650 °C (19–41 days), 700 °C (13–38 days), 800 °C (8–18 days), 900 °C (4–12 days) and 1000 °C (≤9 days) at pressures of 10 and 20 kbar (Table 1). The influence of composition on K_D was studied by performing isothermal reversal runs for 5–6 different garnet compositions. As Fe-rich garnet is more common in nature than Mn-rich varieties, the Fe-side of the system was somewhat emphasized in the experimental investigation.

A general problem encountered in experimental studies involving garnet is the slow rate of cation diffusion in garnet at temperatures <900 °C (Elphick et al. 1985; Chakraborty and Ganguly 1991). Several workers (e.g. Ferry and Spear 1978; Pownceby et al. 1987) circumrouted this problem by using large proportions of garnet relative to the other phase participating in the exchange equilibrium. The bulk composition is then dominated by garnet, and its compositional change in the course of a run is small. The same approach has been adopted here, in that most starting mixtures consisted of 95 wt% garnet and 5 wt% ilmenite (see Table 1 for other mixtures).

Initial experiments at 650 °C and 10 kbar showed that reaction is very minor or not demonstrable at these conditions after run times of three weeks. To promote reaction, 3–10 wt% PbO was added as a flux to the charges at 650 and 700 °C. The PbO was also added to some 800 and 900 °C runs (see Table 1). The oxygen fugacity of the Pb-PbO equilibrium is at slightly lower values than that of the magnetite-hematite buffer (Bannister 1984). Hence PbO was reduced to metallic Pb by the graphite capsule during the experiment. This reduction is visible in the run products as an intergranular Pb film and as small Pb blebs (Fig. 3a–c).

Product characterization

Run products were analyzed by electron microprobe (EMP) using wavelength-dispersive analysis mode. Operation conditions were 15 kV accelerating potential, 20 nA beam current and a beam diameter of ≈1 μm. Counting times of 30–60 seconds were used for Fe, Mn, Al and Si. Titanium was commonly measured during 60 seconds. Standards used included synthetic ilmenite (Fe, Ti), pyrophanite (Mn, Ti), spessartine (Mn, Al, Si), almandine (Fe, Si, Al), rutile (Ti) and natural garnet (Si, Al). Full ZAF corrections were applied to the spectrometer data. The quality and reproducibility of the analyses were monitored by including well-known standards (Fe-Mn ilmenites, garnets, fayalite, tephroite) in the analysis sessions and by regular reanalysis of starting ilmenites and garnets in the same sessions during which the final compositions of the runs were measured. This careful analytical approach was particularly applied in cases where ilmenite composition had changed little during the experiment.

As the products of the dry and PbO-flux exchange experiments at 800–1000 °C consist of a compact garnet-ilmenite mass that can be mounted in epoxy and polished as a whole (Fig. 3), ilmenite and garnet were analyzed at close proximity to each other. Spot analyses in both phases were taken 10–30 μm apart. Using backscattered electron (BSE) imaging mode, 10 to 30 spots in garnet and ilmenite were commonly selected for analysis in each run. Average garnet and ilmenite compositions are listed in Table 1. For 650 and 700 °C experiments, it was not always possible to analyze garnet and ilmenite in contact, as the run products tended to break apart into individual grains during mounting and polishing. In the course of the study, we learnt to preserve the original grain texture largely, by impregnating the run products with epoxy before polishing.

Results

Mineral chemistry of ilmenite and garnet

Whereas starting ilmenites were binary $FeTiO_3$–$MnTiO_3$ solid solutions, final ilmenite may contain up to 4.5 mol% hematite component in solid solution (Fig. 1c). The ferric iron content of ilmenite was calculated from ideal stoichiometry, assuming 2 cations and 3 oxygens per structural formula and considering the components $FeTiO_3$, $MnTiO_3$, $FeSiO_3$, Fe_2O_3 and Al_2O_3. Figure 1c shows that the hematite contents of ilmenite tend to decrease with X_{Mn} for 800–1000 °C runs. Ilmenite from 650 and 700 °C runs does not clearly

Table 1 Experimental parameters and results of runs on Fe-Mn partitioning between garnet and ilmenite. Starting mixtures are in wt%, usually 95% garnet + 5% ilmenite (* 93% garnet + 7% ilmenite, ** 75% garnet + 25% ilmenite). Values *in parentheses* correspond to 1 SD in the digits to their immediate *left*; *n* number of analyses; For final ilmenite: $X_{Mn} = Mn/(Mn + Fe^{2+})$; $X_{Fe^{2+}} = (1 - X_{Mn})$; $X_{Fe^{3+}} = 0.5Fe^{3+}/(0.5Fe^{3+} + Fe^{2+} + Mn + 0.5Al)$; $X_{Al} = 0.5Al/(0.5\,Al + 0.5\,Fe^{3+} + Fe^{2+} + Mn)$; $K_D = [(X_{Mn})\,gnt \cdot (X_{Fe^{2+}})ilm]/[(X_{Fe})gnt \cdot (X_{Mn})ilm]$; *nom* nominal composition (not analysed); † no significant reaction; *tr* trace; Number *in brackets* after *melt* and *Al-spinel* is Mn/Mn + Fe); *metal* is almost pure Fe

Run no.	*P* kbar	*T* °C	Duration days	Starting material		PbO wt%	Final garnet		Final ilmenite				Initial $\ln K_D$	Final $\ln K_D$	Remarks
				X_{Mn} gnt	X_{Mn} ilm		X_{Mn}	*n*	X_{Mn}	$X_{Fe^{3+}}$	X_{Al}	*n*			
25C	20	1000	0.3	0.149(10)	0.100(5)	–	0.152(15)	19	0.098(4)	0.046(6)	0.005	24	0.455	0.501	† Tr melt[0.155], Al-spin[0.060]
1A	20	1000	9	0.250(nom)	0.344(10)	–	0.290(26)	26	0.129(9)	0.018(9)	0.006	28	−0.453	0.979	Tr Al-spin[0.084]
38A**	20	1000	0.3	0.251(26)	0.168(4)	–	0.287(28)	15	0.176(4)	0.035(5)	0.005	19	0.507	0.634	Tr Al-spin[0.113], melt[0.248]
38B**	20	1000	0.3	0.251(26)	0.050(3)	–	0.260(12)	15	0.135(3)	0.038(4)	0.005	20	1.851	0.811	Tr Al-spin[0.068], melt[0.204]
9C	20	1000	4	0.254(9)	0.050(3)	–	0.272(16)	26	0.137(7)	0.028(10)	0.005	33	1.872	0.856	Tr Al-spin[0.085]
23A	10	1000	0.3	0.281(30)	0.050(3)	–	0.321(30)	22	0.173(5)	0.026(6)	0.005	16	2.005	0.815	Tr melt
23B	10	1000	0.3	0.281(30)	0.168(4)	–	0.315(32)	16	0.197(8)	0.036(5)	0.005	24	0.660	0.628	† Tr melt[0.219]
2C*	20	1000	1.5	0.500(nom)	0.408(14)	–	0.539(29)	28	0.309(16)	0.011(7)	0.007	26	0.372	0.961	Tr Al-spin, melt
11A	10	1000	2.7	0.519(11)	0.408(14)	–	0.523(17)	21	0.297(18)	0.007(3)	0.001	9	0.448	0.954	Tr rutile, metal
11B	10	1000	2.7	0.519(11)	0.100(5)	–	0.509(10)	20	0.266(7)	0.000	0.008	15	2.273	1.051	Tr rutile, metal
9A	20	1000	4	0.519(11)	0.408(14)	–	0.527(14)	18	0.278(8)	0.020(4)	0.005	19	0.448	1.063	
9B	20	1000	4	0.519(11)	0.100(5)	–	0.500(11)	20	0.267(10)	0.033(4)	0.005	14	2.273	1.010	
1B	20	1000	9	0.709(18)	0.502(8)	–	0.710(10)	15	0.438(3)	0.003(4)	0.005	14	0.883	1.145	
1C	20	1000	9	0.709(18)	0.168(4)	–	0.697(8)	20	0.427(5)	0.008(7)	0.005	18	2.490	1.127	Tr corundum
23C	10	1000	0.3	0.828(15)	0.502(8)	–	0.833(12)	28	0.614(14)	0.004(6)	0.003	22	1.564	1.143	
11C	10	1000	2.7	0.834(8)	0.707(9)	–	0.825(8)	25	0.583(6)	0.000	0.005	23	0.733	1.216	
25A	20	1000	0.3	0.910(5)	0.697(10)	–	0.915(9)	22	0.754(10)	0.006(7)	0.000	28	1.481	1.256	
25B	20	1000	0.3	0.910(5)	0.797(18)	–	0.918(7)	21	0.779(5)	0.000	0.001	15	0.946	1.156	
21B	20	900	4	0.106(16)	0.050(3)	–	0.101(13)	43	0.033(2)	0.037(6)	0.004	43	0.812	1.192	
21C	20	900	4	0.120(8)	0.000(0)	–	0.125(9)	27	0.039(2)	0.042(7)	0.004	26	∞	1.259	
17A	10	900	4	0.149(10)	0.000(0)	–	0.139(12)	20	0.044(2)	0.045(6)	0.003	23	∞	1.255	
17B	10	900	4	0.149(10)	0.100(5)	–	0.144(13)	21	0.049(2)	0.043(7)	0.003	28	0.455	1.183	
8A	10	900	9	0.254(9)	0.050(3)	–	0.248(4)	18	0.092(4)	0.011(6)	0.004	16	1.872	1.180	
14C	10	900	6	0.255(9)	0.168(4)	–	0.261(11)	21	0.102(3)	0.022(12)	0.003	21	0.528	1.134	
4A*	20	900	9	0.256(10)	0.050(3)	–	0.251(7)	24	0.092(2)	0.041(10)	0.004	20	1.878	1.196	
4B*	20	900	9	0.256(10)	0.168(4)	–	0.264(8)	22	0.102(3)	0.039(13)	0.005	22	0.533	1.150	
42A	20	900	8	0.425(21)	0.302(9)	–	0.424(18)	24	0.185(8)	0.025(8)	0.004	23	0.536	1.176	
4C*	20	900	9	0.500(nom)	0.408(14)	–	0.517(34)	21	0.244(8)	0.012(11)	0.003	21	0.406	1.199	Tr corundum, metal
5A*	20	900	10	0.500(nom)	0.100(5)	–	0.452(27)	30	0.212(12)	0.019(9)	0.003	31	2.004	1.120	Tr metal, quartz
30C	10	900	11	0.515(13)	0.168(4)	–	0.516(16)	24	0.243(3)	0.021(4)	0.002	26	1.660	1.200	
21A	20	900	4	0.515(13)	0.168(4)	–	0.512(15)	17	0.233(4)	0.016(6)	0.002	23	1.660	1.239	
14A	10	900	6	0.543(15)	0.302(9)	–	0.559(11)	17	0.266(6)	0.015(10)	0.003	23	1.010	1.252	
14B	10	900	6	0.543(15)	0.168(4)	–	0.548(14)	21	0.255(6)	0.022(5)	0.003	22	1.772	1.265	
37A	10	900	5	0.709(18)	0.226(2)	–	0.713(18)	15	0.362(5)	0.022(3)	0.002	17	2.122	1.477	
31C	20	900	12	0.726(19)	0.502(8)	–	0.726(9)	27	0.404(6)	0.013(6)	0.001	20	0.966	1.363	Tr rutile, graphite
30B	10	900	11	0.798(13)	0.586(5)	–	0.817(10)	17	0.537(6)	0.013(6)	0.001	18	1.026	1.348	
31B	20	900	12	0.798(13)	0.586(5)	–	0.805(9)	26	0.569(6)	0.018(6)	0.000	23	1.026	1.140	† Tr rutile
42B	20	900	8	0.812(13)	0.707(9)	5	0.813(10)	26	0.541(9)	0.009(4)	0.001	20	0.582	1.305	
42C	20	900	8	0.812(13)	0.397(5)	5	0.807(9)	19	0.534(7)	0.004(6)	0.002	20	1.881	1.294	

Table 1 (continued)

Run no.	P kbar	T °C	Duration days	Starting material		PbO wt%	Final garnet		Final ilmenite				Initial $\ln K_D$	Final $\ln K_D$	Remarks
				X_{Mn} gnt	X_{Mn} ilm		X_{Mn}	n	X_{Mn}	$X_{Fe^{3+}}$	X_{Al}	n			
5B*	20	900	10	0.826(7)	0.302(9)	–	0.797(18)	13	0.444(12)	0.007(6)	0.003	16	2.395	1.593	Tr corundum, rutile
5C*	20	900	10	0.826(7)	0.707(9)	–	0.820(5)	16	0.578(9)	0.009(6)	0.000	17	0.677	1.202	
17C	10	900	4	0.828(15)	0.408(14)	–	0.823(14)	30	0.469(9)	0.009(6)	0.002	22	1.943	1.661	Tr quartz, corundum
30A	10	900	11	0.828(15)	0.502(8)	–	0.834(14)	34	0.520(15)	0.012(6)	0.002	34	1.564	1.534	†
37B	10	900	5	0.828(15)	0.408(14)	4	0.823(9)	17	0.470(6)	0.009(4)	0.001	16	1.944	1.657	
8B	10	900	9	0.834(8)	0.302(9)	–	0.815(15)	15	0.455(11)	0.005(6)	0.000	15	2.452	1.663	Tr corundum
8C	10	900	9	0.834(8)	0.707(9)	–	0.826(8)	21	0.559(8)	0.004(6)	0.000	19	0.733	1.320	Tr corundum
19A	10	800	12	0.106(16)	0.050(3)	–	0.096(14)	22	0.039(2)	0.029(6)	0.001	24	0.812	0.962	
35B	10	800	10	0.106(16)	0.050(3)	4	0.101(10)	16	0.044(1)	0.038(6)	0.001	17	0.812	0.892	†
20A	20	800	12	0.106(16)	0.050(3)	–	0.107(19)	21	0.042(4)	0.036(10)	0.002	27	0.812	1.005	
36C	20	800	8	0.106(16)	0.050(3)	4	0.106(12)	16	0.038(2)	0.044(6)	0.001	19	0.812	1.099	
20B	20	800	12	0.120(8)	0.000(0)	–	0.127(8)	18	0.041(4)	0.036(3)	0.002	19	∞	1.225	
35C	10	800	10	0.120(10)	0.000(0)	4	0.127(8)	23	0.036(1)	0.038(6)	0.001	16	∞	1.360	
41B	20	800	13	0.120(8)	0.100(5)	5	0.129(8)	22	0.040(2)	0.041(5)	0.001	20	0.205	1.268	
22C	10	800	13	0.247(13)	0.100(5)	–	0.259(13)	26	0.108(4)	0.000	0.001	28	1.083	1.060	†
28B	10	800	14	0.247(13)	0.050(3)	3	0.255(11)	23	0.094(6)	0.000	0.002	26	1.830	1.194	
28C	10	800	14	0.247(13)	0.168(4)	3	0.259(13)	25	0.105(2)	0.000	0.001	25	0.486	1.092	rutile lamellae in ilmenite
36B	20	800	8	0.247(13)	0.168(4)	4	0.268(8)	18	0.113(2)	0.002(6)	0.001	20	0.485	1.056	
3A*	20	800	10	0.256(10)	0.050(3)	–	0.250(7)	32	0.085(6)	0.026(11)	0.002	24	1.878	1.278	
3B*	20	800	10	0.256(10)	0.168(4)	–	0.257(8)	28	0.103(3)	0.013(9)	0.002	18	0.533	1.103	
13A	10	800	9	0.281(30)	0.050(3)	–	0.270(18)	20	0.075(4)	0.024(5)	0.000	21	2.001	1.518	
13B	10	800	9	0.281(30)	0.168(4)	–	0.292(28)	20	0.128(3)	0.018(8)	0.001	22	0.660	1.033	
7C	20	800	12	0.425(21)	0.302(9)	–	0.416(25)	26	0.165(5)	0.020(5)	0.002	25	0.536	1.282	Tr corundum, quartz
3C*	20	800	10	0.500(nom)	0.100(5)	–	0.458(21)	20	0.191(3)	0.015(6)	0.002	23	2.197	1.275	
22A	10	800	13	0.515(15)	0.168(4)	–	0.517(22)	38	0.235(7)	0.023(9)	0.001	35	1.660	1.248	
22B	10	800	13	0.515(15)	0.302(9)	–	0.530(20)	27	0.245(7)	0.020(13)	0.001	20	0.898	1.246	
10A	10	800	10	0.519(11)	0.408(14)	–	0.521(13)	18	0.259(7)	0.013(6)	0.002	16	0.448	1.135	
10B	10	800	10	0.519(11)	0.100(5)	–	0.504(8)	19	0.194(5)	0.023(7)	0.001	17	2.273	1.440	
41A	20	800	13	0.630(9)	0.502(8)	5	0.634(6)	20	0.359(5)	0.021(4)	0.000	24	0.524	1.129	
29C	20	800	18	0.726(19)	0.302(9)	4	0.721(14)	21	0.358(10)	0.009(6)	0.000	17	1.812	1.533	Some rutile lamellae in ilmenite
19C	10	800	12	0.798(13)	0.408(14)	–	0.803(12)	17	0.450(10)	0.012(6)	0.000	20	1.746	1.606	
28A	10	800	14	0.798(13)	0.408(14)	5	0.797(14)	31	0.459(9)	0.022(5)	0.000	24	1.746	1.532	Some rutile lamellae in ilmenite
20C	20	800	12	0.798(13)	0.586(5)	–	0.808(16)	22	0.517(9)	0.014(8)	0.000	18	1.026	1.369	Tr rutile
29A	20	800	18	0.798(13)	0.408(14)	3	0.793(12)	23	0.464(10)	0.017(8)	0.000	19	1.746	1.487	Some rutile lamellae in ilmenite
35A	10	800	10	0.812(13)	0.586(5)	4	0.811(12)	17	0.503(7)	0.010(7)	0.000	24	1.116	1.445	Tr rutile
41C	20	800	13	0.812(13)	0.586(5)	5	0.810(11)	24	0.519(10)	0.012(5)	0.000	24	1.116	1.374	Tr rutile
7A	20	800	12	0.826(7)	0.302(9)	–	0.808(10)	14	0.347(3)	0.000	0.000	13	2.395	2.069	Tr rutile, quartz
10C	10	800	10	0.834(8)	0.707(9)	–	0.826(8)	22	0.565(5)	0.013(6)	0.001	15	0.733	1.296	Tr corundum
13C	10	800	9	0.834(8)	0.302(9)	–	0.824(11)	11	0.349(12)	0.000	0.001	10	2.452	2.167	

Table 1 (continued)

Run no.	P kbar	T °C	Duration days	Starting material		PbO wt%	Final garnet		Final ilmenite				Initial $\ln K_D$	Final $\ln K_D$		Remarks
				X_{Mn} gnt	X_{Mn} ilm		X_{Mn}	n	X_{Mn}	$X_{Fe^{3+}}$	X_{Al}	n				
33C	10	700	18	0.120(10)	0.000	5	0.125(8)	19	0.021(1)	0.024(5)	0.000	17	∞	1.896		
40A	10	700	26	0.120(8)	0.020(1)	10	0.123(9)	15	0.020(1)	0.025(4)	0.000	19	1.899	1.927	†	
40B	10	700	26	0.120(8)	0.050(3)	10	0.129(8)	26	0.032(1)	0.018(4)	0.000	23	0.952	1.500		
40C	10	700	26	0.247(13)	0.050(3)	10	0.249(9)	20	0.056(1)	0.000	0.000	16	1.830	1.721		Tr rutile in ilmenite
33A	10	700	18	0.259(13)	0.100(5)	5	0.260(10)	20	0.084(3)	0.015(8)	0.000	22	1.097	1.343		
33B	10	700	18	0.259(13)	0.050(3)	5	0.258(16)	19	0.063(2)	0.019(6)	0.000	26	1.846	1.643		
43C	10	700	38	0.259(13)	0.100(5)	10	0.261(9)	22	0.088(2)	0.018(5)	0.000	28	1.146	1.298		
32A	10	700	13	0.497(10)	0.226(2)	5	0.512(10)	22	0.213(3)	0.012(8)	0.000	20	1.219	1.355		
32B	10	700	13	0.515(14)	0.168(4)	5	0.514(12)	21	0.189(3)	0.022(5)	0.000	17	1.660	1.513		
43A	10	700	38	0.630(9)	0.226(2)	10	0.625(9)	22	0.252(4)	0.017(6)	0.000	22	1.763	1.599		
43B	10	700	38	0.630(9)	0.302(9)	10	0.635(10)	14	0.299(3)	0.009(7)	0.000	17	1.370	1.406	†	
34C	10	700	26	0.726(19)	0.397(5)	5	0.729(10)	18	0.359(5)	0.016(5)	0.000	23	1.392	1.569		
39B	10	700	25	0.726(19)	0.302(9)	10	0.735(10)	15	0.309(5)	0.011(6)	0.000	20	1.812	1.825	†	
34A	10	700	26	0.810(12)	0.502(8)	5	0.819(10)	19	0.486(8)	0.018(7)	0.000	22	1.442	1.566		
39A	10	700	25	0.812(13)	0.502(8)	10	0.815(10)	15	0.444(10)	0.019(5)	0.000	14	1.442	1.708		
39C	10	700	25	0.812(13)	0.397(5)	10	0.812(13)	19	0.419(6)	0.013(5)	0.000	18	1.881	1.790	†	
34B	10	700	26	0.828(15)	0.408(14)	5	0.834(15)	20	0.434(5)	0.008(7)	0.000	20	1.944	1.880	†	Tr rutile
18A	10	650	21	0.106(16)	0.050(3)	–	0.090(29)	4	0.044(2)	0.010(15)	0.000	12	0.812	0.946		
18B	10	650	21	0.106(16)	0.000(0)	–	0.089(23)	5	0.010(3)	0.005(11)	0.000	6	∞	2.463		
26A	10	650	41	0.120(10)	0.050(3)	3	0.129(8)	29	0.036(2)	0.011(7)	0.000	31	0.952	1.378		
27A	10	650	21	0.120(10)	0.000(0)	4	0.125(5)	17	0.018(2)	0.013(7)	0.000	18	∞	2.053		
18C	10	650	21	0.247(13)	0.100(5)	–	0.248(10)	19	0.083(3)	0.000	0.000	21	1.083	1.293		
12A	10	650	26	0.281(30)	0.050(3)	–	0.279(31)	24	0.072(2)	0.015(6)	0.000	24	1.995	1.610		Tr Al-spin [0.072]
12B	10	650	26	0.281(30)	0.168(4)	–	0.295(35)	19	0.143(3)	0.011(9)	0.000	17	0.660	0.919		Tr Al-spin [0.071]
12C	10	650	26	0.507(10)	0.100(5)	–	0.523(14)	21	0.137(5)	0.013(5)	0.000	22	2.225	1.933		
15C	10	650	24	0.515(13)	0.168(4)	–	0.516(14)	24	0.181(4)	0.017(7)	0.000	35	1.660	1.574	†	
27B	10	650	21	0.515(13)	0.226(2)	4	0.527(17)	19	0.224(5)	0.017(10)	0.000	14	1.291	1.351	†	
27C	10	650	21	0.515(13)	0.168(4)	4	0.522(16)	17	0.181(5)	0.019(7)	0.000	25	1.660	1.598	†	
24A	10	650	19	0.543(15)	0.226(2)	3	0.544(12)	16	0.220(3)	0.007(8)	0.000	22	1.404	1.442	†	
24B	10	650	19	0.726(19)	0.397(5)	5	0.741(19)	10	0.304(8)	0.000	0.000	18	1.392	1.879		
24C	10	650	19	0.726(19)	0.226(2)	4	0.731(10)	21	0.255(5)	0.000	0.000	24	2.205	2.072		
15A	10	650	24	0.798(13)	0.302(9)	–	0.809(12)	25	0.336(6)	0.009(5)	0.000	24	2.212	2.125	†	
15B	10	650	24	0.798(13)	0.408(14)	–	0.802(16)	13	0.413(17)	0.005(6)	0.000	29	1.746	1.750	†	
26C	10	650	41	0.910(5)	0.586(5)	5	0.919(11)	15	0.605(9)	0.004(7)	0.000	23	1.966	2.002	†	

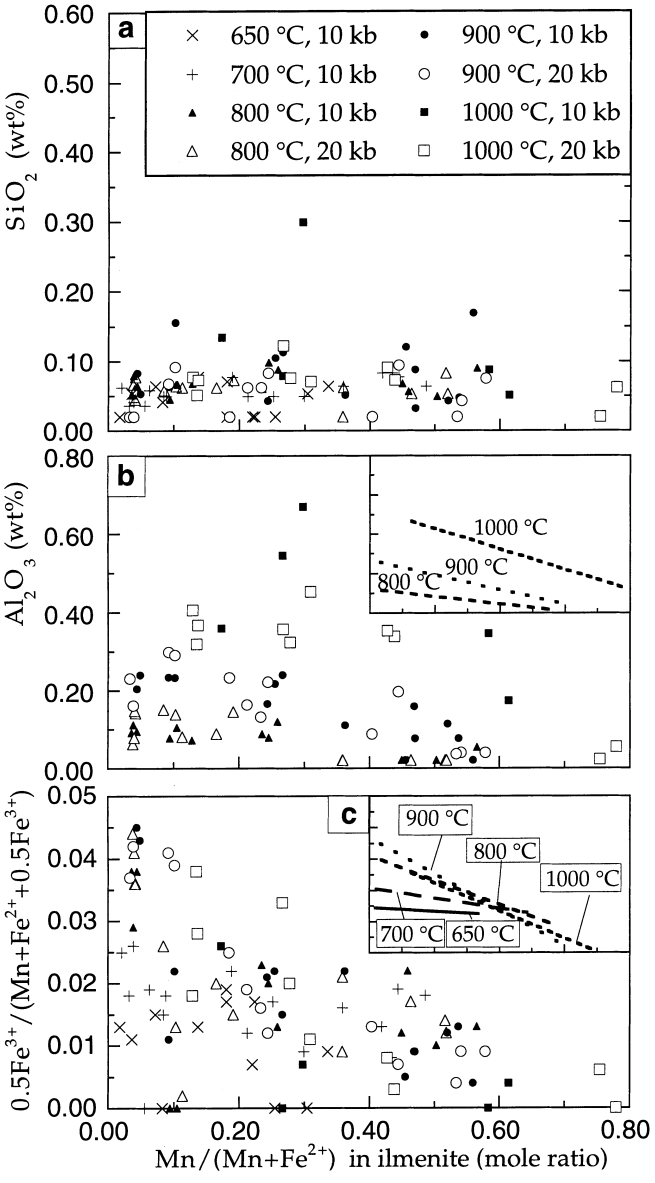

Fig. 1a–c Chemical variation of ilmenite in exchange runs. *Symbols* represent averages of probe analyses for each experiment (cf., Table 1): **a** SiO_2 versus X_{Mn}; **b** Al_2O_3 versus X_{Mn}. *Inset* shows trends at 800, 900 and 1000 °C. Al_2O_3 in ilmenite was below detection limit for 650 and 700 °C runs. **c** Hematite contents versus X_{Mn}. The *inset* shows isothermal trends

display such a relationship and is characterized by hematite contents of <2.6 mol%.

Ilmenite contains <0.30 wt% SiO_2 and <0.67 wt% Al_2O_3 (Fig. 1a, b). The Al_2O_3 contents increase with temperature: at 650 and 700 °C ilmenite contains no detectable Al_2O_3 (≈0.02 wt%); at 800 °C Al_2O_3 is <0.15 wt% ($X_{Al} \leq 0.002$). At 900 and 1000 °C, the Al_2O_3 contents of ilmenite range up to 0.30 wt% ($X_{Al} \leq 0.005$) and 0.67 wt% ($X_{Al} \leq 0.008$), respectively (Fig. 1b; Table 1). The very minor SiO_2 contents of ilmenite show a tendency to increase slightly with temperature (Fig. 1a).

Garnet analyses were normalized to 12 oxygens, assuming all iron is ferrous. Calculated formulae are very close to $^{VIII}(Fe^{2+},Mn)_3{}^{VI}Al_2{}^{IV}(Si,Al)_3O_{12}$ stoichiometry (Fig. 2b), pointing to negligible ferric iron in garnet. This fits in with the low hematite contents of coexisting ilmenite and indicates fairly low oxygen fugacities prevailing during the exchange experiments. The Si contents of garnet range from 2.90 to 3.04 atoms per formula unit (pfu), with most garnets showing slight deficiencies in silica (Fig. 2a). This may be related to the fact that garnet did not coexist with quartz in our experiments, although slight Si-deficiencies are not unusual for natural aluminosilicate garnet saturated in SiO_2 either. The TiO_2 in garnet is below or near detection limit in the 650 °C runs and increases with temperature to as much as 1.0 wt% TiO_2 in the 1000 °C runs. As will be discussed in a subsequent section, the TiO_2 contents of garnet measured near ilmenite are largely an analytical artifact, resulting from secondary fluorescence effects.

Chemical homogeneity of run products

To test for chemical zoning in ilmenite and garnet, traverses across ilmenite grains and adjacent garnets (up to 300 μm long) were measured in 10 runs by EMP step scans. Representative compositional profiles are shown for each experimental temperature in Fig. 4. Ilmenite is unzoned at all experimental conditions. Garnet is zoned only with respect to Ti, with the (apparent) TiO_2 contents clearly increasing towards ilmenite contacts. Such a zoning pattern was observed in all runs studied; its significance is discussed below.

In some parts of the garnet profiles, erratically high TiO_2 values were measured, particularly at the higher temperatures (Fig. 4d and f). These higher values are ascribed to submicroscopic ilmenite (or rutile) inclusions (partly occurring below the polished surface) which were included in the garnet analyses.

Ti-zoning of garnet: predominantly an analytical artifact

The possibility that the titanium zoning displayed by garnet in contact with ilmenite is caused by edge or secondary fluorescence effects should be considered (e.g., Maaskant and Kaper 1991; Reed 1993; Dalton and Lane 1996). To test for this, a garnet-ilmenite couple was constructed. Polished surfaces of garnet ($X_{Mn} = 0.124$) and ilmenite ($X_{Mn} = 0.020$) chips, both mounted in epoxy, were glued together, with ≈1 μm gap between the phases. Several traverses (up to 140 μm long) were measured across the interface, at analytical conditions identical to those applied analyzing the run products. Titanium was measured using a PET crystal on a spectrometer with a take-off angle of 40°. A step size of 1 μm was used for the traverses.

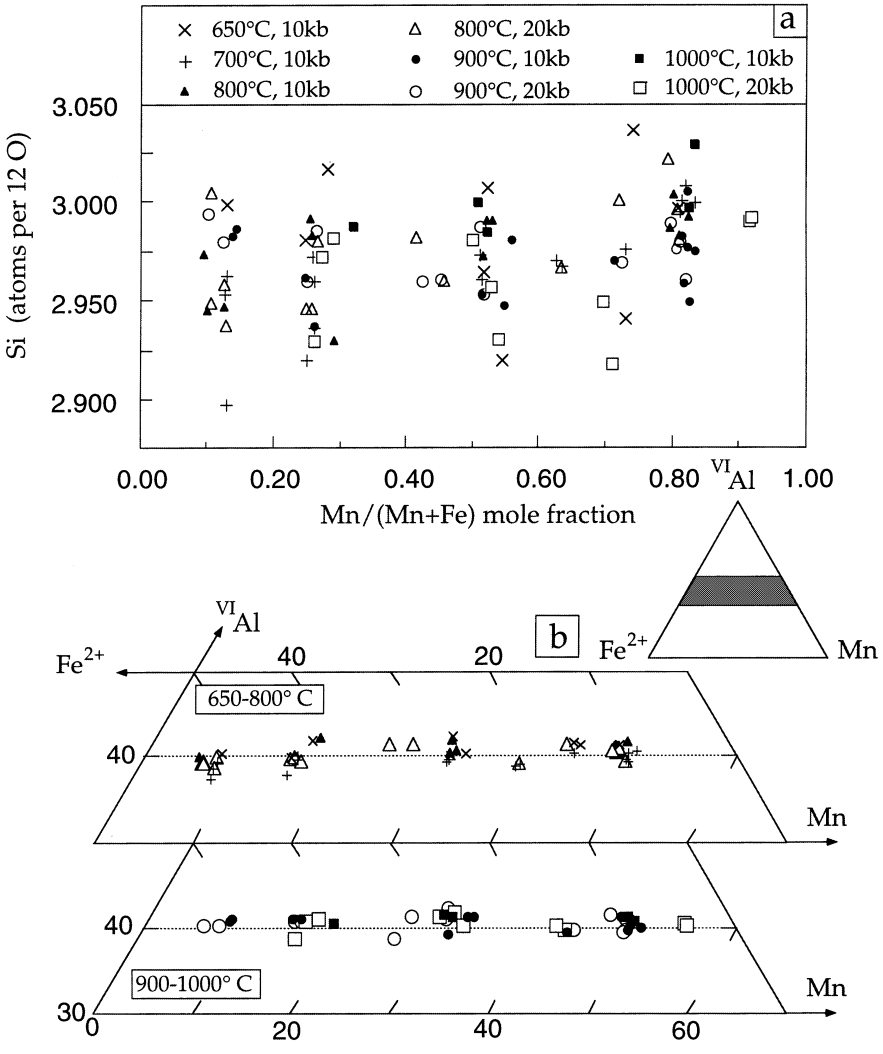

Fig. 2a–b Chemical variation of garnet in exchange runs. *Symbols* represent averages of spot analyses for each experiment largely performed some 5–10 microns from grain contact with ilmenite (cf., Table 1). For 650 and 700 °C runs it was not always possible to measure garnet in close distance from ilmenite (see text). Total iron is expressed as ferrous. **a** Si versus X_{Mn}; **b** Molar Fe^{2+}-Mn-^{VI}Al diagram. (^{VI}Al total Al + Si − 3.0 for Si < 3.0, ^{VI}Al total Al for Si ≥ 3.0)

A representative traverse across the garnet-ilmenite couple (Fig. 5) illustrates that garnet, which contains no titanium, has an apparent Ti content up to a distance of ≈50 μm away from the interface. Zoning for other elements was not found in any traverse, neither in garnet nor ilmenite. The slight decrease for all major elements in garnet at the interface is interpreted to result from the fact that here the beam excitation volume is partly in the ≈1 μm wide interface gap. The apparent TiO_2 contents in the garnet 10 μm from the interface are ≈0.45 wt%, ≈0.20 wt% at 20 μm, then the Ti-counts gradually drop to the detection limit (≈0.05 wt%) at ≈50 μm.

The highest Ti concentrations in garnet, within a few microns from ilmenite, are likely due to a combination of edge effects and secondary fluorescence. The former are related to the fact that the volume excited by the electron beam is still partly inside ilmenite, where primary Ti-K_α radiation is generated. The latter effect is predominantly due to Ti-K_α fluorescence generated by Fe-K_α (and Mn-K_α) radiation in garnet. This is not corrected for by the ZAF program. At the applied experimental conditions (15 kV, 20 nA beam current), the beam interaction volume should be exclusively within one phase for a distance of >3–4 μm from the interface (e.g. Ganguly et al. 1988; Reed 1993). Therefore, the Ti-zoning pattern in garnet beyond that range must be a consequence of secondary fluorescence. Maaskant and Kaper (1991) describe similar effects in the analysis of ilmenite-hematite pairs and Dalton and Lane (1996) in the analysis of olivine in contact with Ca-rich phases. These workers pointed out that secondary fluorescence may lead to erroneous thermobarometric results.

The apparent Ti-zoning pattern in garnet of the garnet-ilmenite couple is very similar to the patterns measured in run products (cf. Fig. 4), though more irregular in the latter. This is probably a consequence of the less regular interface geometry (in 3D) between ilmenite and garnet. Some of the flatter Ti-zoning patterns may indicate a true TiO_2 content in garnet near ilmenite, but the apparent TiO_2 content still includes a superimposed portion due to fluorescence. Inspection of Fig. 4 shows that titanium in garnet does not decrease below detection limit in any of the traverses studied,

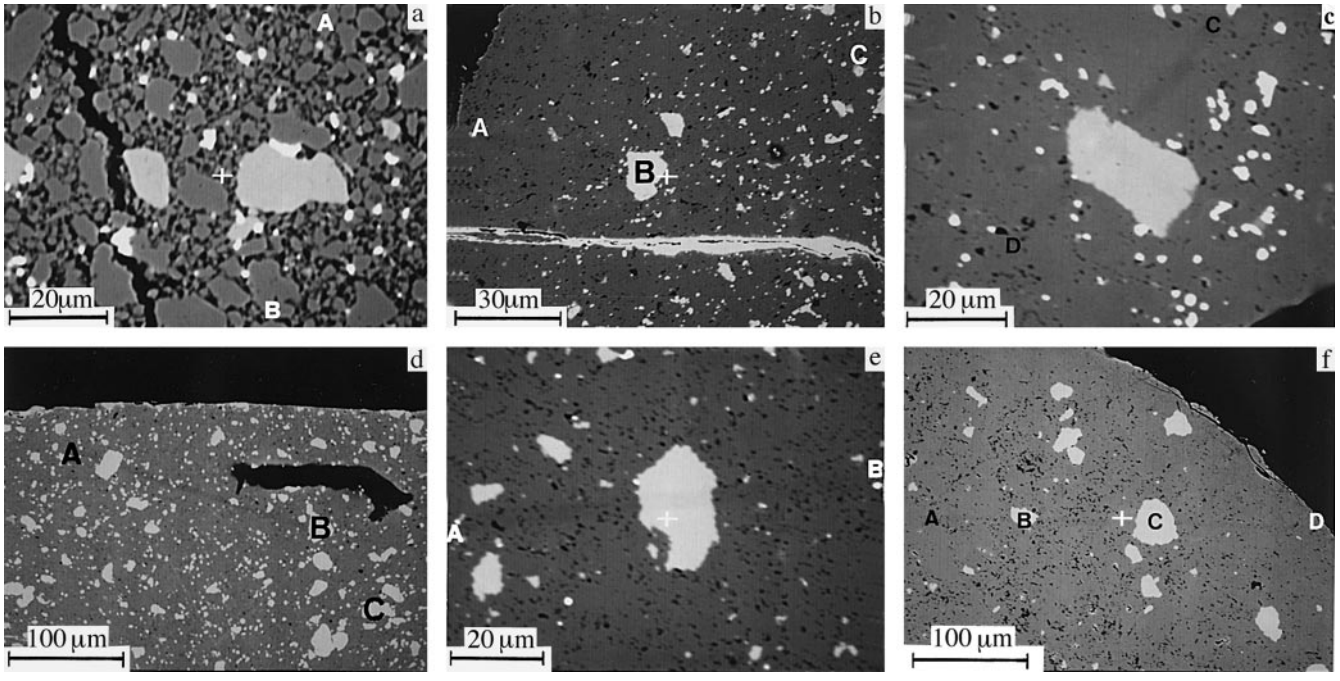

Fig. 3a–f Back-scattered electron images of garnet-ilmenite Fe-Mn exchange experiments. *Dark grey* matrix is garnet, *medium grey* grains are ilmenite and *small white rounded* grains in **a**, **b** and **c** are Pb-flux. *Capitals* on photographs indicate positions of electron microprobe traverses shown in Fig. 4. Garnet subgrains are vaguely mirrored by *dark zones* (holes) due to poorer polish at grain boundaries. **a** Run GP32B, 700 °C, 10 kbar, 13 days, 5% PbO flux added; **b** run GP29A, 800 °C, 20 kbar, 18 days, 3% PbO flux added; **c** run GP41C, 800 °C, 20 kbar, 13 days, 5% PbO flux added; **d** run GP4B, 900 °C, 20 kbar, 9 days; **e** run GP21A, 900 °C, 20 kbar, 4 days; **f** run GP1B, 1000 °C, 20 kbar, 9 days

even though some analyzed spots are >50 μm away from ilmenite. However, these observations are difficult to interpret because the Ti patterns may reflect ilmenite grains that lay below or above the polished surface. The unknown geometry of the ilmenite-garnet grain boundaries, together with the fact that the influence of composition on the intensity of secondary fluorescence (cf. Dalton and Lane 1996) cannot be evaluated because only one (Fe-rich) garnet-ilmenite couple was studied, hamper successful discrimination between Ti occurring in the garnet lattice and apparent Ti content.

In summary, our data suggest that the Ti-zoning patterns measured in garnet of the run products are predominantly artificial, a consequence of secondary Ti fluorescence in ilmenite. There is a tendency for the average Ti content (typically measured at 5–15 μm distance from ilmenite) to increase with temperature. For the high-T runs the fluorescence-induced Ti-counts in garnet may be superimposed on true Ti contents established by diffusion during the experiments. On the basis of all the analytical work done in this study, the true TiO_2 contents of garnet are estimated to be <0.4 wt% even at 1000 °C, and probably <0.2 wt% at 800 °C.

Fe-Mn partitioning between garnet and ilmenite

As indicated by fairly narrow experimental brackets (Fig. 6), exchange equilibrium between ilmenite and garnet has been closely approached by most of the 800–1000 °C runs. Reversals at 650 and 700 °C (and the most Mn-rich compositions at 800 and 900 °C) give wider experimental brackets. We tried to reduce the width of brackets in subsequent runs by adding 3–10 wt% PbO-flux to the reactants and by choosing starting compositions of Fe-Mn ilmenite fairly close to the expected equilibrium compositions (yet far enough to permit an unambiguous determination of the reaction direction). The EMP analysis showed that PbO in ilmenite was below detection limit (<0.10 wt%) for all runs. Garnet of 700 and 800 °C runs is free of Pb but garnet of the three 900 °C PbO-fluxed runs does contain up to 0.60 wt% PbO. Only in a few runs the grain size of the flux, which was reduced to metallic Pb, was sufficient to permit EMP analysis. The results show that the flux is fairly pure Pb, with Fe + Mn < 1.50 wt%.

In some experiments at 1000 °C special problems were encountered. These include the partial or complete reduction of ilmenite to metallic Fe + rutile, and the formation of small fractions of melt in runs of Fe-rich composition. Due to the partial melting and concomitant formation of Fe-Mn-Al spinel (Table 1), ilmenite and garnet became enriched in manganese, resulting in unreliable reversal data. The problem of ilmenite reduction could largely be solved by decreasing the run times. We attempted to prevent partial melting by taking special care to dry the reactants when filling the capsules (whereas in all other cases no precaution was taken to avoid moisture). Nevertheless, at 1000 °C and 10 kbar,

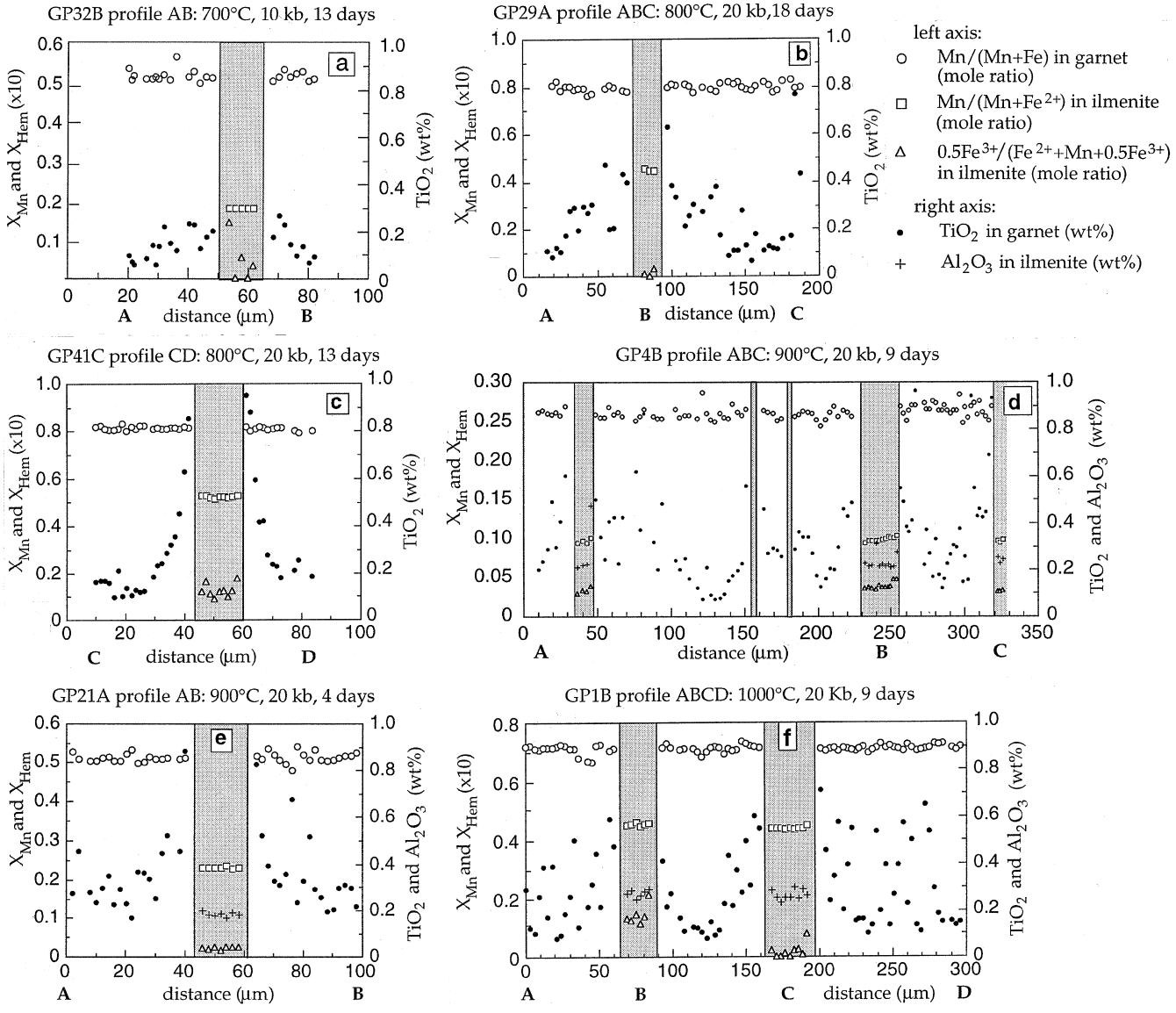

Fig. 4a–f Electron microprobe step scans of run products at 700, 800, 900, and 1000 °C. Refer to corresponding micrographs in Fig. 3. *Horizontal scale* of shorter profiles (**a**, **c**, **e**) is expanded twice with respect to longer profiles (**b**, **d**, **f**). Mole fraction of Mn in garnet shows approximately flat profiles as do mole fractions of Mn and hematite in ilmenite. Note homogeneous distribution of Al_2O_3 in ilmenite grains (Al_2O_3 in ilmenite was below detection limit in **a**, **b** and **c**) and conspicuous zoning of TiO_2 in garnet close to ilmenite (discussed in text). The scatter of TiO_2 concentrations in **d** and **f** may be due to finely dispersed submicroscopic ilmenite grains included in the garnet spot analyses

the most Fe-rich compositions yielded so much melt (5–15%) that these experiments were ignored in the data analysis.

Discussion

Comparison with previous studies

Figure 6 compares our experimental results for equilibrium (1) with those of Kress (1986) and Pownceby et al. (1987) in X_{Mn} garnet versus $\ln K_D$ diagrams. Arrows connect initial to final $\ln K_D$ values. Box sizes for our data reflect estimated uncertainties in X_{Mn} garnet and $\ln K_D$. These are based on 1 standard deviation in X_{Mn} (X_{Fe}) of garnet and ilmenite as determined by EMP (cf. Table 1), assuming a minimum uncertainty of 0.01 in X_{Mn}^{gnt} and 0.001–0.010 in X_{Mn}^{ilm} (M. Engi and A. Feenstra, in preparation). The magnitude of the latter was approximated as: $0.04 * X_{Mn}^{ilm} * (1 - X_{Mn}^{ilm})$. Box sizes in Fig. 6 thus correspond to the 1σ values of our multiple probe data, except where this variation was less than the minimum uncertainties quoted above, in which case these minimum values are plotted.

Pownceby et al. (1987) did not report compositional variation for their product ilmenite and garnet, whereas Kress (1986) gave only compositional variation of final ilmenite. For this reason, half-brackets of both studies are simply shown by arrows connecting initial and final $\ln K_D$. We estimate, however, that compositional uncertainties of final garnet and ilmenite in these earlier

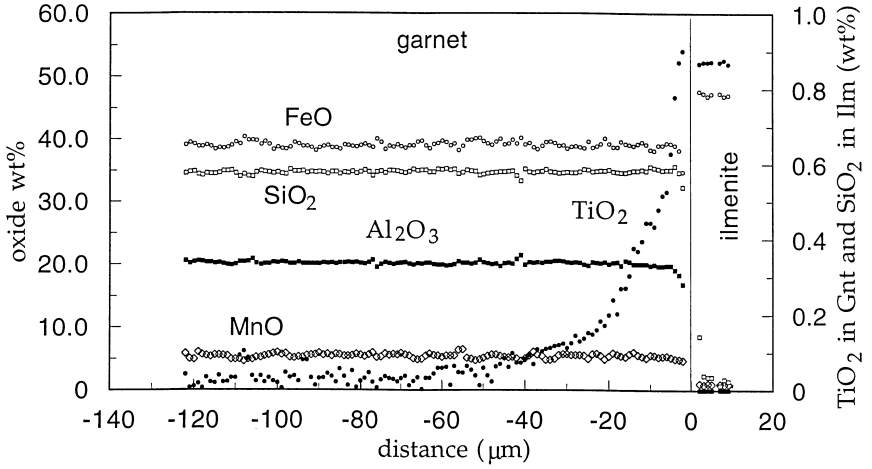

Fig. 5 Electron microprobe step scan across a couple of garnet ($X_{Mn} = 0.124$) and ilmenite ($X_{Mn} = 0.020$) constructed by gluing together Ti-free garnet and Al- and Si-free ilmenite. Garnet-ilmenite boundary was oriented vertically for microprobe analysis. Apparent TiO_2 contents of garnet and SiO_2 contents of ilmenite are plotted on the *right* axis, all other oxides on the *left* axis. Al_2O_3 contents of ilmenite were below detection limit in all analyses. Analytical conditions used: 15 kV accelerating potential, 20 nA beam current, beamsize ≈1 μm, 50 seconds counting time for Ti, 10 s on background (PET crystal, spectrometer take-off angle 40°), all other elements 30 s on peaks with 5 s on background, full ZAF corrections made (PAP program, CAMECA software)

studies are approximately of similar magnitude as in the present one.

The data depicted in Fig. 6 cover a *P-T* range from 2–20 kbar and 600–1000 °C. As already noted by Pownceby et al. (1987), the Fe-Mn partitioning between garnet and ilmenite is hardly dependent on pressure, being in line with the very small $\Delta_r V^0 = -0.021$ J/bar of reaction (1) (M. Engi and A. Feenstra, in preparation). For comparative purposes in Fig. 6, the effect of pressure on K_D can be neglected for the experimental data shown.

Ilmenite (and garnet) changed very little in composition in several of our experiments. On the basis of compositional uncertainty for ilmenite and garnet as discussed above, it was decided whether or not such experiments yielded significant changes in K_D and hence contribute information on the direction of reaction (cf. Table 1). Pownceby et al. (1987) also reported several runs with minor compositional changes. However, that study fails to provide detailed information on compositional homogeneity of final garnet and ilmenite, making it difficult to judge whether $\ln K_D$ at the end is significantly different from that at the start of the experiment, the more so as starting $\ln K_D$ is inexactly known (garnet in starting mixture was assumed to be of nominal composition). Based on our own findings, we arbitrarily decided that $\ln K_D$ changes of < 0.10 are inconclusive for the reaction direction (such runs are not shown in Fig. 6.) A $\Delta \ln K_D$ confidence interval of ± 0.10 is deemed adequate for intermediate garnet compositions; for very Fe or Mn rich compositions, where $\ln K_D$ is rather sensitive to small changes in ilmenite and garnet composition, larger $\ln K_D$ changes may be required to determine unambiguously the direction of reaction (cf. our data in Fig. 6).

Inspection of Fig. 6 shows that, taking into account uncertainties in $\ln K_D$, virtually all our results are in agreement with the previous studies of Kress (1986) and Pownceby et al. (1987). It is obvious, however, that we were able to constrain $\ln K_D$ more tightly than in the previous studies, particularly for Mn-rich compositions. It is also clear that, contrary to Pownceby et al. (1987), who have interpreted $\ln K_D$ to be independent of composition, our brackets indicate that $\ln K_D$ is significantly larger for Mn-rich garnets than for Fe-rich ones. This compositional dependence of $\ln K_D$ seems to exist at all experimental temperatures. Furthermore, Fig. 6 provides evidence that for Fe-rich compositions $\ln K_D$ may be less dependent on temperature than Pownceby et al. (1987) had assumed.

Three half-brackets of Kress (1986) for Mn-rich compositions at 900 °C (marked by asterisks in Fig. 6b) are clearly inconsistent with the other data. Kress (1986) reports much higher hematite contents of ilmenite (5.8–10.6 mole% Fe_2O_3 for his 900 °C runs) than would be expected at the conditions of his experiments (f_{O_2} was buffered by IW). We suggest that such oxidized ilmenite compositions may be an artifact due to inaccurate EMP analysis. Overestimated hematite contents will profoundly affect K_D values at Mn-rich compositions and strongly displace K_D to lower values there.

Concluding remarks

The present study emphasizes the importance of detailed EMP work in characterizing reactants and products of exchange experiments. Such EMP data provide information on the chemical homogeneity of phases in the experiments, which is essential for assigning uncertainty limits to final K_D and, in the case of minor compositional changes, to decide whether or not significant reaction has occurred. The EMP traverses measured

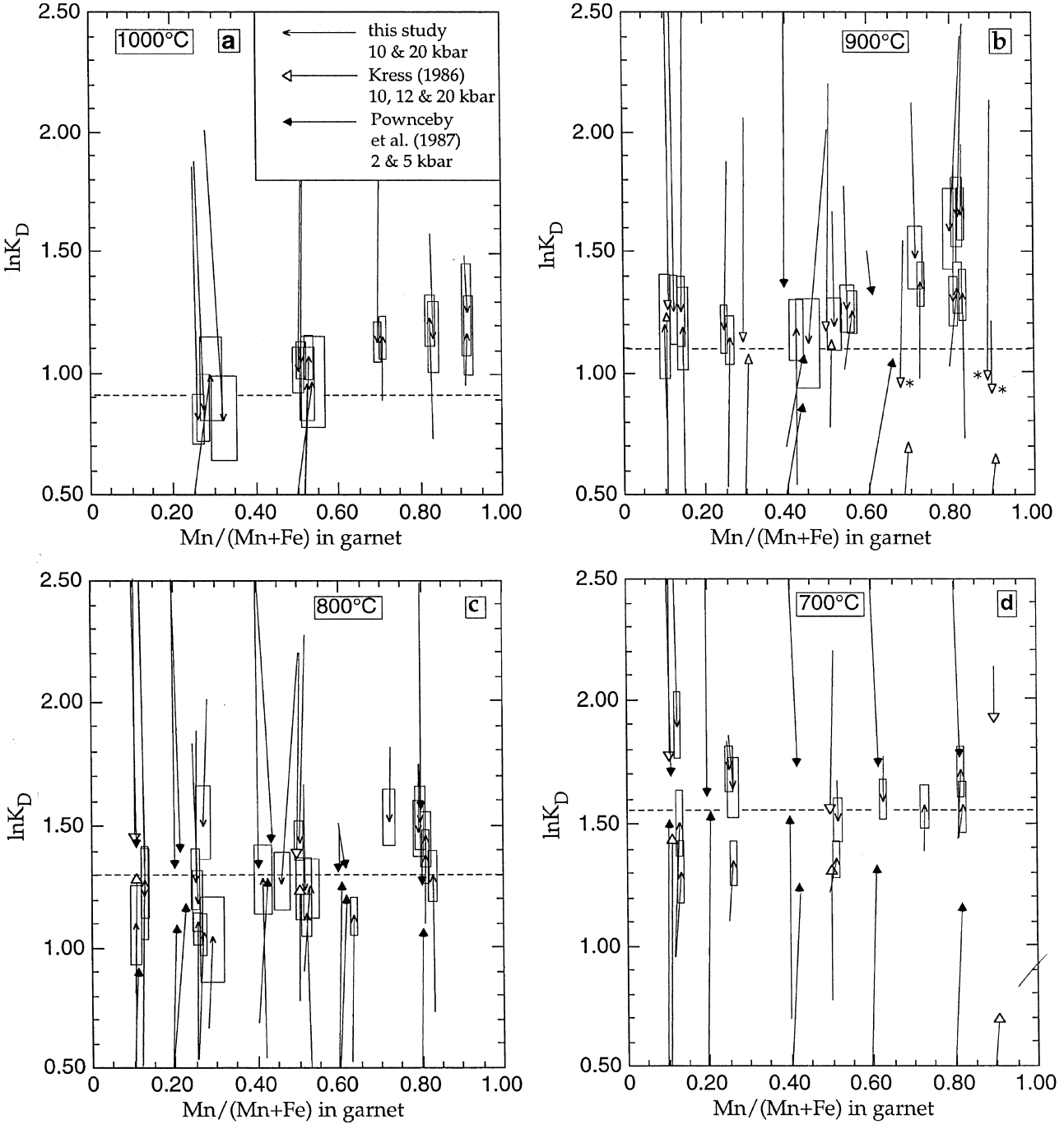

Fig. 6a–e Variation of $\ln K_D \left[= (X_{Mn}^{gnt} \cdot X_{Fe}^{ilm})/(X_{Fe}^{gnt} \cdot X_{Mn}^{ilm}) \right]$ with X_{Mn} ratio of garnet for Fe-Mn exchange experiments. Start and final $\ln K_D$ values are shown by *arrows*. *Box sizes* for data of present study reflect uncertainties in final X_{Mn}^{gnt} and $\ln K_D$, whereas uncertainties are not shown for half-brackets of Kress (1986) and Pownceby et al. (1987) (see text and Table 1). Three half-brackets of Kress (1986), marked by *asterisks* (**b**), disagree with the other data (see text). *Dashed horizontal lines* depict $\ln K_D$ as deduced by Pownceby et al. (1987) from their experimental study (their Eq. 7). For clarity, several less constraining half-brackets of Pownceby et al. (1987) and present study have not been displayed in the figures

across ilmenite grains and adjacent garnet show that both phases are unzoned in X_{Mn} (X_{Fe}) but also reveal a predominantly artificial Ti-zoning in garnet up to ≈40–50 μm away from the garnet-ilmenite interface. High apparent Ti contents are caused by secondary Ti-fluorescence of ilmenite, as was demonstrated by analyzing profiles across a couple constructed from ilmenite and Ti-free garnet.

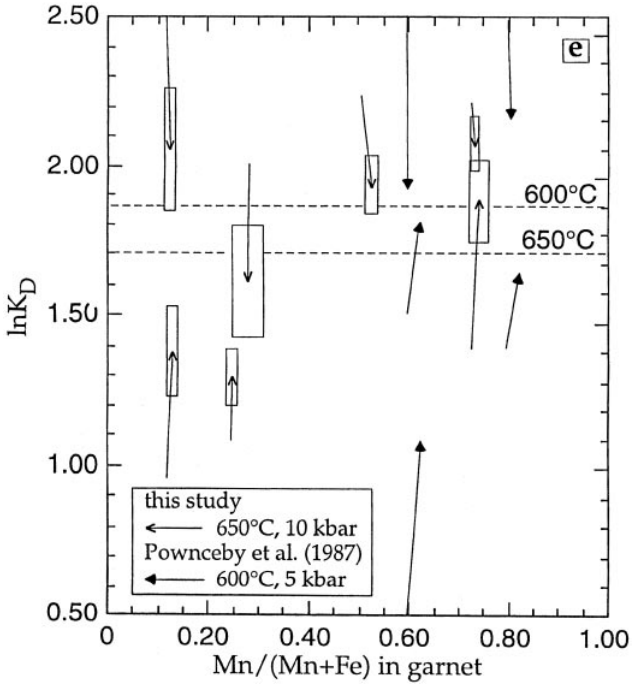

Virtually all results of three experimental studies on the Fe-Mn partitioning between garnet and ilmenite (Kress 1986; Pownceby et al. 1987; this study) are consistent with each other. Only a few results of Kress (1986) disagree with the other data. As explained above, we question the EMP data for ilmenite from that study. Contrary to the previous studies, however, the narrow experimental brackets obtained during the present calibration constrain that, at constant temperature, K_D is larger for Mn-rich compositions than for Fe-rich ones. This compositional dependence of K_D complicates garnet-ilmenite geothermometry. For geothermometric application, it is unfortunate that results for Fe-rich compositions (X_{Mn} garnet $< \approx 0.25$), which dominate in nature, will not be very accurate. This is owing to a lesser T-dependence of K_D at Fe-rich compositions (cf. Fig. 6) as well as less precise K_D values connected to small mole fractions of X_{Mn}, particularly in ilmenite. Best results from garnet-ilmenite thermometry are expected to be obtained at intermediate compositions ($\approx 0.25 < X_{Mn}$ garnet $< \approx 0.80$).

Thermodynamic analysis of the Fe-Mn garnet-ilmenite partitioning data, together with other experimental data in the system Fe-MnO-Al_2O_3-TiO_2-SiO_2-O_2 (M. Engi and A. Feenstra, in preparation), indicates that $(Fe,Mn)_3Al_2Si_3O_{12}$ garnets deviate more strongly from ideality than proposed till now (nearly ideal). This nonideal Mn mixing extends into multicomponent garnet solution models as well.

Acknowledgements We thank Rob Berman and Tjerk Peters for helpful discussions. We also gratefully acknowledge critical comments of an anonymous reviewer and Jibamitra Ganguly in particular, who helped to shape the content of this paper. The study was financially supported by the "Schweizerischer Nationalfonds" (grants 20-29921.90 and 20-40623.94); this foundation also supported the Cameca SX-50 electron microprobe of the University of Bern (grant 21-26579.89).

References

Bannister MJ (1984) The standard molar Gibbs free energy of formation of PbO. Oxygen concentration-cell measurements at low temperatures. J Chem Thermodyn 16: 787–792

Berman RG (1990) Mixing properties of Ca-Mg-Fe-Mn garnets. Am Mineral 75: 328–344

Berman RG, Aranovich LY (1996) Optimized standard state and mixing properties of minerals. I. Model calibration for olivine, orthopyroxene, cordierite, garnet, and ilmenite in the system FeO-MgO-CaO-Al_2O_3-SiO_2-TiO_2. Contrib Mineral Petrol 126: 1–24

Berman RG, Koziol AM (1991) Ternary excess properties of grossular–pyrope–almandine garnet and their influence in geothermobarometry. Am Mineral 76: 1223–1231

Bohlen SR, Wall VJ, Boettcher AL (1983) Experimental investigations and geologic applications of equilibria in the system FeO-TiO_2-Al_2O_3-SiO_2-H_2O. Am Mineral 68: 1049–1058

Chakraborty S, Ganguly J (1991) Compositional zoning and cation diffusion in garnets. In: Ganguly J (ed) Diffusion, atomic ordering and mass transport. (Advances in physical geochemistry, vol 8) Springer-Verlag, Berlin Heidelberg New York Tokyo, pp 120–175

Dalton JA, Lane SJ (1996) Electron microprobe analysis of Ca in olivine close to grain boundaries: the problem of secondary X-ray fluorescence. Am Mineral 81: 194–201

Docka JA (1984) Ilmenite-garnet Mn-Fe exchange: calibration from naturally occurring pairs (abstract). Geol Soc Am Abstr Program 16: 491

Elphick SC, Ganguly J, Loomis TP (1985) Experimental determination of cation diffusivities in aluminosilicate garnets. 1. Experimental methods and interdiffusion data. Contrib Mineral Petrol 90: 36–44

Essene E (1989) The current status of thermobarometry in metamorphic rocks. In: Daly JS, Cliff RA, Yardley BWD (eds) Evolution of metamorphic belts. Blackwell Scientific Publications, Oxford, pp 1–44

Feenstra A, Peters Tj (1996) Experimental determination of activities in $FeTiO_3$-$MnTiO_3$ ilmenite solid solution by redox reversals. Contrib Mineral Petrol 126: 109–120

Ferry JM, Spear FS (1978) Experimental calibration of the partitioning of Fe and Mg between biotite and garnet. Contrib Mineral Petrol 66: 113–117

Ganguly J, Saxena SK (1984) Mixing properties of aluminosilicate garnets: constraints from natural and experimental data, and applications to geothermo barometry. Am Mineral 69: 88–97

Ganguly J, Bhattacharya RN, Chakraborty S (1988) Convolution effect in the determination of compositional profiles and diffusion coefficients by microprobe step scans. Am Mineral 73: 901–909

Ganguly J, Cheng W, Tirone M (1996) Thermodynamics of aluminosilicate garnet solid solution: new experimental data, an optimized model, and thermometric applications. Contrib Mineral Petrol 126: 137–151

Gavrieli I, Matthews A, Holland TJB (1996) Ca-Mn exchange between grossular and $MnCl_2$ solutions at 2 kbar and 600°C: reaction mechanism and evidence for non-ideal mixing in spessartine–grossular garnets. Contrib Mineral Petrol 125: 251–262

Geiger CA, Feenstra A (1993) A study of synthetic almandine–spessartine garnets: ^{57}Fe Mössbauer spectroscopy and molar volumes of mixing. Abstract EUG VII Strasbourg (abstract). TERRA nova Suppl 5: 489

Geiger CA, Feenstra A (1997) Molar volumes of mixing of almandine–pyrope and almandine–spessartine garnets and the crystal chemistry and thermodynamic mixing properties of aluminosilicate garnets. Am Mineral 82: 571–581

Geiger CA, Newton RC, Kleppa OJ (1987) Enthalpy of mixing of synthetic almandine–grossular and almandine–pyrope garnets from high-temperature solution calorimetry. Geochim Cosmochim Acta 51: 1755–1763

Hackler RT, Wood BJ (1989) Experimental determination of Fe and Mg exchange between garnet and olivine and estimation of Fe-Mg mixing properties in garnet. Am Mineral 74: 994–999

Johannes W (1978) Pressure comparing experiments with NaCl, AgCl, talc and pyrophyllite assemblies in a piston-cylinder apparatus. Neues Jahrb Mineral Monatsh 1978: 84–92

Koziol AM (1990) Activity-composition relationships of binary Ca-Fe and Ca-Mn garnets determined by reversed, displaced equilibrium experiments. Am Mineral 75: 319–327

Koziol AM (1996) Quaternary (Ca-Fe-Mg-Mn) garnet: displaced equilibrium experiments and implications for current garnet mixing models. Eur J Mineral 8: 453–460

Koziol AM, Bohlen SR (1992) Solution properties of almandine–pyrope garnet determined by phase equilibrium experiments. Am Mineral 77: 765–773

Koziol AM, Newton RC (1989) The activity of grossular in ternary (Ca, Fe, Mg) garnet determined by reversed phase equilibrium experiments at 1000 and 900 °C. Contrib Mineral Petrol 103: 423–433

Kress VC (1986) Iron-manganese exchange in coexisting garnet and ilmenite (unpublished). MSc thesis, State Univ New York

Maaskant P, Kaper H (1991) Fluorescence effects at phase boundaries: petrological implications for Fe-Ti oxides. Mineral Mag 55: 277–279

Ono A (1980) Partitioning of Fe and Mn between garnet and ilmenite: an experimental study. J Jpn Assoc Mineral Petrol Econ Geol 75: 160–163

Pownceby MI, Wall VJ, O'Neill HStC (1987) Fe-Mn partitioning between garnet and ilmenite: experimental calibration and applications. Contrib Mineral Petrol 97: 116–126

Pownceby MI, Wall VJ, O'Neill HStC (1991) An experimental study of the effect of Ca upon garnet-ilmenite Fe-Mn exchange equilibria. Am Mineral 76: 1580–1588

Reed SJB (1993) Electron microprobe analysis, 2nd edn. Cambridge Univ Press, Cambridge

Spear FS (1993) Metamorphic phase equilibria and pressure-temperature-time paths. Mineral Soc Am Monogr, Washington, DC

Tracy RJ (1982) Compositional zoning and inclusions in metamorphic minerals. In: Ribbe PH (ed) Characterization of metamorphism through mineral equilibria. (Reviews in mineralogy, vol 10) Mineral Soc Am, Washington, DC, pp 355–397

Tracy RJ, Robinson P, Thompson AB (1976) Garnet composition and zoning in the determination of temperature and pressure of metamorphism, central Massachusetts. Am Mineral 61: 762–775

Wood BJ, Hackler RT, Dobson DP (1994) Experimental determination of Mn-Mg mixing properties in garnet, olivine and oxide. Contrib Mineral Petrol 115: 438–448

Woodsworth GJ (1977) Homogenization of zoned garnets from pelitic schists. Can Mineral 15: 230–242